Journal of Alloys and Compounds 584 (2014) 369–373

Contents lists available at ScienceDirect

Journal of Alloys and Compounds

journal homepage: www.elsevier.com/locate/jalcom

# Investigations on structure, ferroelectric, piezoelectric and energy storage properties of barium calcium titanate (BCT) ceramics

Venkata Sreenivas Puli [a,*], Dhiren K. Pradhan [b], Brian C. Riggs [a], Douglas B. Chrisey [a], Ram S. Katiyar [b]

[a] Department of Physics and Engineering Physics, Tulane University, New Orleans, LA 70118, USA
[b] Department of Physics and Institute for Functional Nanomaterials, University of Puerto Rico, San Juan, PR 00936, USA

ARTICLE INFO

*Article history:*
Received 13 August 2013
Received in revised form 14 September 2013
Accepted 16 September 2013
Available online 24 September 2013

*Keywords:*
BCT
Aging
Ferroelectrics
Energy density
Solid state sintering

ABSTRACT

We investigated structural, aging induced ferroelectric, piezoelectric and energy density properties of ceramic $(Ba_{0.70}Ca_{0.30})TiO_3$ (BCT) capacitors that were prepared by the solid-state reaction method. According to X-ray (XRD) data, along with $BaTiO_3$ tetragonal peaks, $CaTiO_3$ rich orthorhombic peaks were also observed at room temperature. Raman scattering gives evidence for the formation of oxygen vacancies in BCT due to partial migration of $Ca^{2+}$ into $Ti^{4+}$ site. Abnormal double like hysteresis polarization-electric field ($P$–$E$) loops were observed at room temperature for naturally aged BCT ceramics. Strain-electric field ($S$–$E$) loops confirm piezoelectric behavior. Room temperature (300 K) charge curve and discharge curve energy densities [$(Ed)_c \sim 0.35$ (before aging) 0.39 J/cm$^3$ (aged)], [$(Ed)_d \sim 0.20$ (before aging) 0.24 J/cm$^3$ (aged)], respectively, at a maximum electric field ~50 kV/cm. The bulk BCT materials have shown interesting energy densities with good energy storage efficiency (~58% before aging, ~61% after aging) suggesting they might be strong candidates for high energy density capacitor applications.



## 1. Introduction

Barium titanate ($BaTiO_3$ or BT)-based materials have been extensively studied for their interesting electrical properties like high dielectric constant, low dielectric loss, ferroelectric, piezoelectric and pyroelectric behavior. Among the dielectric ferroelectric perovskite oxides, BT was used most for electrical and electronic applications, in the years immediately after its discovery. Perovskite oxides derived from BT have a wide range of applications in electronic appliances, such as positive temperature coefficient devices, pulse generating devices, infrared detectors, voltage tunable devices in microwave electronics, multilayer ceramic capacitors, actuators, and lead-free piezoelectric transducers, and charge storage devices [1,2]. Recently, research attention turned towards lead-free and environmentally-friendly dielectric $BaTiO_3$ based piezoelectric materials because of its high dielectric constant, polarization and high piezoelectric properties [3]. BT based high dielectric constant materials with low dielectric loss and high dielectric breakdown field are useful in energy storage capacitors.

Doping is an effective way to improve the electrical performance of electroceramics [4,5]. For instance, barium zirconium titanate $Ba(Zr,Ti)O_3$ [BZT], and barium calcium titanate $(Ba,Ca)TiO_3$ [BCT] [4–6,8] are widely used in electrical material applications. Also, these materials are attracting attention as ceramic capacitors in which the temperature dependence and reliability of the dielectric properties of the BT are improved [6,7]. BCT solid solutions are specifically used in multilayer ceramic capacitor applications and in various other applications like: dielectric filters, antennas, resonators, duplexers and phase shifters, and piezoelectric actuators [8]. $Ca^{2+}$ can occupy either $Ba^{2+}$ site or $Ti^{4+}$ site in $BaTiO_3$ lattice. $Ca^{2+}$ substitution in the $Ti^{4+}$ site requires charge compensation by creating oxygen vacancies in $Ba(Ca_xTi_{1-x})O_{3-x}$ [7]. However the site occupancy mechanism in $BaTiO_3$ is still not completely understood. Ca is known to have solubility upper limit of $x \sim 25$ mol.% on A site doping and an upper limit of $x \sim 4$ mol.% on B-site doping in $BaTiO_3$ [9,10]. Oxygen vacancies are created by charge compensation mechanism and this might be the reason for $Ca^{2+}$ (ionic radius $r_{Ca} = 0.99$ Å) occupancy at B-site ($Ti^{4+}$ site, ionic radius of $r_{Ti} = 0.60$ Å) in perovskite $BaTiO_3$. The solubility limit of $Ca^{2+}$ occupying B-site ($x \sim 0.04$) in $Ba(Ca_xTi_{1-x})O_3$ [11], is much lower when compared to that of A-site doping, due to the larger ionic radius of $Ca^{2+}$ to that of $Ti^{4+}$ [7].

Aging induced double $P$–$E$ hysteresis behavior has been previously observed for lead-free perovskite $BaTiO_3$/$(Ba,Sr)TiO_3$ [12], $BiFeO_3$ [13], $KNbO_3$ [14], and $(Na,Bi)TiO_3$-based ceramics [15]. However, not much was reported on BCT ceramics aging behavior and only a few reports were available on $Ca^{2+}$ occupying $Ti^{4+}$ in $BaTiO_3$ lattice with aging behavior [16–19]. Many studies are available on BCT based materials for capacitor applications; but none were found on energy density measurements to our knowledge. Many studies are available on BCT based materials for capacitor

* Corresponding author. Tel.: +1 239 537 4964; fax: +1 504 862 8702.
*E-mail addresses:* vpuli@tulane.edu, pvsri123@gmail.com (V.S. Puli).

0925-8388/$ - see front matter © 2013 Elsevier B.V. All rights reserved.
http://dx.doi.org/10.1016/j.jallcom.2013.09.108

applications; but none were found on energy density measurements to our knowledge. Here in, we report structure, Raman spectra, ferroelectric, piezoelectric and energy density measurement of BCT ceramics for capacitor applications.

### 2. Experimental procedure

High-purity $BaCO_3$ (99%), $CaCO_3$ (99%), $TiO_2$ (98%) (Alfa Aesar, U.S.A) powders were used as the starting materials. $(Ba_{0.70}Ca_{0.30})TiO_3$ ceramics were prepared by the conventional solid state reaction of $BaCO_3$, $CaCO_3$ and $TiO_2$. Stoichiometric quantities of starting materials were ball-milled in a polyethylene jar for 4 h using $ZrO_2$ balls with ethanol. The mixtures were heated at 800 °C in air for 3 h after drying and sieving. The mixture was calcined at 1250 °C for 10 h. The calcined powder was ball milled and dried again to obtain homogeneous powder. The granulated powders were pressed into disks of 13 mm in diameter and 0.5 mm in thickness using 5% PVA binder, binder burnt out by heating at 500 °C for 1 h and then sintered at 1500 °C in air for 6 h. X-ray diffraction (XRD) patterns at room temperature were obtained on an automated Rigaku D/max 2400 X-ray diffractometer with rotating anode using Cu Kα radiation. After polishing, the dimensions were measured before silver electrodes were deposited on the pellets, then the specimens were fired at 810 °C for 1 h. The Raman measurements were performed using an ISA T64000 triple monochromator. An optical microscope with an 80× objective was used to focus 514.5 nm radiations from a Coherent Innova 99 argon ion laser on the sample. Laser power of ~10 mW was focused on a ~2 μm spot. The same microscope objective collected the backscattered radiation. The scattered light, dispersed by the spectrophotometer, was detected by using a 1 inch charge-coupled device (CCD) detection system with 1800 grooves/mm grating and the spectral resolution was typically <1 $cm^{-1}$. Ferroelectric hysteresis loops was measured at 50 Hz, with poled disk-shaped samples under an electric field using Radiant Technologies high voltage amplifier (RT 6000 HVA-4000V). Dielectric breakdown voltage of the samples was measured at room temperature using a Trek high voltage amplifier (Trek Inc., Model 30kV/20A).

### 3. Results and discussion

Fig. 1 shows the room temperature XRD patterns obtained from $(Ba_{0.70}Ca_{0.30})TiO_3$ (BCT) ceramics with angle $2\theta$ (degree) ranging from 10° to 80° with a scan rate of 1° per minute. Tetragonal peaks corresponding to perovskite $BaTiO_3$ and orthorhombic peaks corresponding to $CaTiO_3$ XRD patterns were observed for BCT ceramics with majority of tetragonal phase peaks as reported in previous investigations [20–24] and tetragonal BCT, XRD reflection peaks are isostructural with $Ba_{0.88}Ca_{0.12}TiO_3$ (JCPDS 81-1288). In addition to prominent indexed tetragonal diffraction peaks, orthorhombic peaks corresponding to $CaTiO_3$ were detected at $2\theta = 32.94°$, 47.43°, 58.87°, 69.07° and were indexed with (121), (202), (042) planes respectively. Detected peaks are isostructural with $CaTiO_3$ in complete agreement with JCPDS 75-2100 [24,25]. According to the phase diagram of $BaTiO_3$–$CaTiO_3$ solid solutions prepared by conventional dry route, the formation of $CaTiO_3$ is expected for $x \geqslant 0.16$ at the calcination temperature of 1150 °C [23,26]. In the present study, prolonged calcination (1250 °C/10 h) and sintering (1350 °C/4 h) could not suppress the orthorhombic phase for higher concentrations of calcium in BCT (not shown here). Whereas sintering at higher temperature ~1500 °C/6 h, drastically reduced orthorhombic peaks and whose lattice parameters [($a \sim 3.95191$ Å, $c \sim 3.94950$), tetragonal distortion ($c/a \sim 0.99$) and volume (~61.6817 $Å^3$)] of the unit cell decreased from that of the lower sintering temperature 1350 °C/4 h, [($a \sim 3.958$ Å, $c \sim 4.066$ Å), tetragonal distortion ($c/a \sim 1.027$) and volume (~63.7094 $Å^3$)]. This decrease might be due to partial incorporation of calcium at barium site due to higher sintering temperature (1500 °C) with more dwelling time (6 h). The SEM micrographs of BCT ceramics are shown in Fig. 1 inset. It is found that the sintered ceramics are very dense, uniform void free. The average grain size of the ceramics calculated by line intercept method is around 40–65 μm.

Ferroelectric tetragonal $BaTiO_3$ contain 3A1 + B1 + 4E Raman active phonons; however cubic phase has no Raman active modes in $BaTiO_3$. In brief, room temperature tetragonal $BaTiO_3$ Raman mode were $E(TO_1)$, $A_1(TO_1)$ [sharp mode ], $A_1(TO_2)$ [asymmetric broad mode ], $B_1/E(TO + LO)$ [sharp mode],$A_1(TO_3)/E(TO_2)$ [asymmetric broad mode], $A_1(LO)/E(LO)$ [asymmetric broad mode]. However much broader and symmetrical [$A_1(TO_2)$, $A_1(TO_3)/E(TO)$, $A_1(LO)/E(LO)$] modes are also present in cubic paraelectric phase, they were often attributed to second-order effects. More precisely, they relate to the disorder of Ti displacements in the $TiO_6$ octahedra [10]. Raman spectrum in Fig. 2, reveals spectral features at 146 $cm^{-1}$ [$A_1(TO_1)$], 224 $cm^{-1}$ [$A_1(TO_2)$], 297 $cm^{-1}$ [$B_1/E(TO + LO)$], 473 $cm^{-1}$ $A_1(LO_2)/E(LO)$], 524 $cm^{-1}$ [$A_1(TO_3)/E(TO)$], 734 $cm^{-1}$ [$A_1(LO)/E(LO)$], 863 $cm^{-1}$ [$A_{1g}$]. Similar results were observed in $Ba_{(1-x)}Ca_xTiO_3$, $BaTi_{(1-x)}Ca_xO_3$ ceramic systems [16,27]. The shift of the modes namely [$A_1(TO_3)/E(TO)$, $A_1(LO)/E(LO)$] to higher frequencies when compared to pure and Ca substituted $BaTiO_3$ [27], implies an increase in force constant which resulted from the presence of higher amount of calcium in reaction at the Ba sites. Also the shift of these bands to higher frequencies is attributed to the formation of $Ca_{Ba}$ defects, which is closely related to the phonon vibrations of the Ba–O bonds [27]. Both [$A_1(TO_2)$], [$B_1/E(TO + LO)$] modes at 224 $cm^{-1}$ and 297 $cm^{-1}$ respectively shifted towards lower wave number region, the shift in these two bands to lower wave number region might be caused by the phonon vibrations of Ti–O bonds [27].

These results are in agreement with previous reports on $BaTiO_3$, $Ba_{(1-x)}Ca_xTiO_3$ (BCT), $BaTi_{(1y)}Ca_yO_3$ (BTC) [16,17,27] and simulta-

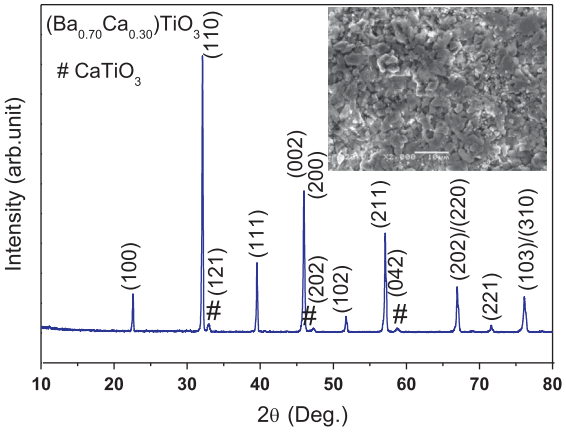


**Fig. 1.** Room temperature (300 K) slow-scan XRD patterns of $(Ba_{0.70}Ca_{0.30})TiO_3$ (BCT) with $2\theta$ angle ranging 20–80°, scanning electron microscopy image of BCT ceramics (inset).

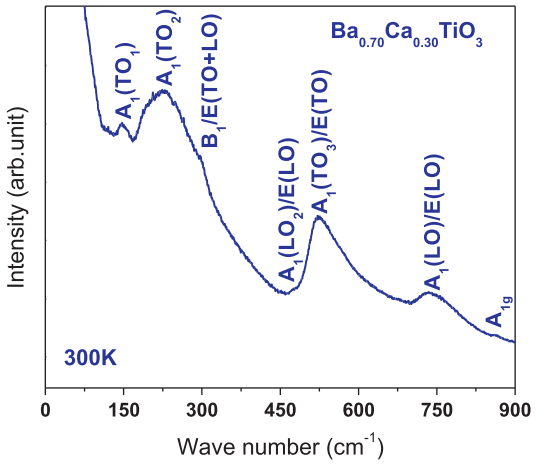


**Fig. 2.** Room temperature (300 K) unpolarized Raman spectra of $(Ba_{0.7}Ca_{0.3})TiO_3$ – (BCT) ceramics with phonon mode assignments.

neously substituted $La^{3+}$, $Yb^{3+}$ system in $BaTiO_3$ [34]. In contrary to these results, Strathdee et al., reported that [$A_1(TO_2)$] mode shifted to higher wave number region, when both $Bi^{3+}$ and $Yb^{3+}$ simultaneously incorporated into the $BaTiO_3$ lattice [35]. This is attributed to the presence of lone pair electrons in $Bi^{3+}$, which hardens the phonon vibrations in $BaTiO_3$–$BiYbO_3$ system and as well as the bond bending in Ti–O bonds in $TiO_6$ octahedra [17,35].

In general the presence of $B_1$/E(TO + LO), $A_1(TO_3)$/E(TO) modes represents the tetragonal phase at room temperature. Strong $A_{1g}$ octahedral breathing mode is only observed in BTC ceramics, which is Raman inactive for simple perovskite structured materials, and this mode is observed when $Ca^{2+}$ is substituted for $Ti^{4+}$ in $BaTiO_3$ lattice [10]. This higher wave number Raman mode has resulted from the formation of $Ca_{Ti}$ defects. Extended X-ray absorption fine structure (EXAFS) results on $BaTi_{0.97}Ca_{0.03}O_{2.97}$ (BTC) solid solutions revealed that the Ca occupancy on the Ti site is only 2% instead of 3%. The remaining 1% of Ca occupied Ba site [31].

Raman spectra of present BCT ceramics, revealed a well defined breathing mode ($A_{1g}$) peak at 863 $cm^{-1}$ whereas this peak was absent in the spectra of $BaTiO_3$, (Ba,Ca)$TiO_3$ in earlier reports [10,32]. Presence of $A_{1g}$ mode in BCT ceramics might be attributed to the greater amount of $Ca^{2+}$ on the $Ba^{2+}$ (A) site than its solid solubility limit and as well we predict that $Ca^{2+}$ ions partially migrated into both $Ba^{2+}$ and as well as $Ti^{4+}$ sites due to solid solubility limit $x = 0.25$ [31]. As well previous reports also supports that some of the $Ca^{2+}$ ion have been substituted for the $Ti^{4+}$ ions, even when the chemical composition of the starting materials with the ratio of A-site ions to B-site ions was one for BCT [16,33]. And as well presence of octahedral breathing mode ($A_{1g}$) is also attributed due to the formation of oxygen vacancies at both $Ba^{2+}$ and $Ti^{4+}$ sites due to partial migration of $Ca^{2+}$ from $Ba^{2+}$ to $Ti^{4+}$ site. This may imply that, the $Ca^{2+}$ ion is partially substituted for $Ti^{4+}$ in BCT ceramics, and $O^{2-}$ vacancies have formed to compensate for the charge imbalance [16,19,27]. Almost similar results were evidenced in $Ca^{2+}$ ion substitution for B-site $Ti^{4+}$ ions has in Bi–BCT [16,27].

The *P–E* loops were examined using a computer controlled modified Sawyer–Tower circuit operating at a frequency of 50 Hz. BCT ceramics were poled overnight (~20 kV/cm) and then ferroelectric measurements were carried out. The ferroelectric nature of conventionally prepared BCT ceramics was confirmed by a hysteresis loop of polarization (*P*) as a function of applied electric field (*E*) with a maximum electric field of 50 kV/cm, before and after aging. Before aging BCT samples have shown normal ferroelectric hysteresis loops. Abnormal double hysteresis *P–E* loops were observed at room temperature for naturally aged (3 weeks) samples. *P–E* hysteresis loops of the conventionally prepared BCT ceramics were shown in Fig. 3 (a). The saturation polarizations ($P_s$) were ~16.78 μC/$cm^2$ (before aging) and 17.53 μC/$cm^2$ (after aging), remnant polarization ($P_r$) ~ 4.37 μC/$cm^2$ (before aging) and 2.25 μC/$cm^2$ (after aging), the coercive field ($E_c$) ~ 9.10 kV/cm (before aging) and 5.12 kV/cm (after aging) respectively for of the BCT ceramics were shown in Fig. 3(a) and Table 1.

Single hysteresis *P–E* loops become double-like in the *P–E* hysteresis behavior after natural aging for 3 weeks demonstrating antiferroelectric like behavior. However, such double hysteresis loop behavior is only found when $Ca^{2+}$ ions occupies $Ti^{4+}$ site in BCT ceramics [16,17]. The aging effect with double hysteresis *P–E* loop behavior in acceptor-doped ferroelectrics is generally considered to be caused by the migration of oxygen vacancies (which are highly mobile) during aging in Bi–BCT samples and as well the ground state of Bi-doped $(Ba_{1-x}Ca_{x/2}Sr_{x/2})TiO_3$ (BCST) might be antiferroelectric at about 6 °C [17–19]. The spontaneous polarization values for aged BCT are comparably higher than before aging; however the remnant polarization and coercive field values are behave in opposite manner and are less pronounced after aging. The present BCT ceramics exhibit comparatively improved values in

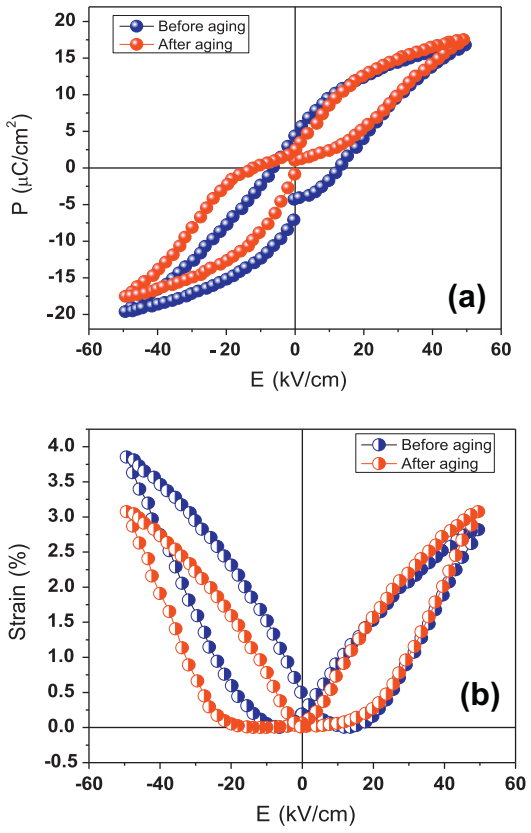


**Fig. 3.** Room temperature. (a) Polarization-field (*P–E*) loops (before and after aging). (b) Strain-field (*S–E*) loops (before and after aging) of $(Ba_{0.7}Ca_{0.3})$ $TiO_3$ – (BCT) ceramics sintered at 1500 °C at 50 Hz.

both cases (before aging and after aging) than earlier reports [16,17]. Presence of such an antiferroelectric double hysteresis *P–E* loop behavior might be attributed to oxygen vacancies created during partial migration of $Ca^{2+}$ from $Ba^{2+}$ site to $Ti^{4+}$ site in perovskite $BaTiO_3$ as explained earlier. Asymmetric *S–E* piezoelectric butterfly hysteresis loops were observed in both cases (before aging and after aging) as shown in Fig. 3(b). Electric field dependent strain behavior in both cases (before and after aging) reveals that obvious nonlinear transition region is observed in bi-polar region of the measurement that corresponds to the possible steps of the reorientation of domains induced by external electric fields [4,28]. The aged BCT ceramics exhibited a little higher maximum percentage of strain (~3%) than the normal samples (~2.8%) at ~50 kV/cm). BCT ceramics have shown higher strain than pure $BaTiO_3$ ceramics (~0.14% at 50 kV/cm) [4], as well as $Ba_{0.77}Ca_{0.23}$-$TiO_3$ ceramics (~0.22% at 50 kV/cm) [21].

The energy density (*Ed*) of a capacitor is calculated from the *P–E* hysteresis loop, and is the integral area of the *P–E* loop (charge-

**Table 1**
Room temperature remnant polarization ($P_r$), spontaneous polarization ($P_s$) and coercive field ($E_c$) of *P–E* loops and piezoelectric properties (strain maximum%, and degree of hysteresis of ($\Delta x/x$)%) of remnant polarization-$P_r$, Saturation polarization-$P_s$, Coercive field ($E_c$), Strain maximum% ($S_{max}$%), Degree of hysteresis ($\Delta x/x$%), of $(Ba_{0.7}Ca_{0.3})$ $TiO_3$ – (BCT) ceramics.

| Composition $(Ba_{0.70}Ca_{0.30})TiO_3$ | $P_r$ (μC/$cm^2$) | $P_s$ (μC/$cm^2$) | $E_c$ (kV/cm) | $S_{max}$ % | Degree of hysteresis ($\Delta x/x$) % |
|---|---|---|---|---|---|
| Before aging | 4.37 | 16.73 | 9.10 | 2.8 | 47 |
| After aging | 2.25 | 17.53 | 5 12 | 3.0 | 42 |

**Table 2**
Room temperature dielectric breakdown field and discharge energy density $(Ed)_d$, charge energy density $(Ed)_c$ and energy storage efficiency ($\eta$%) of $(Ba_{0.7}Ca_{0.3})TiO_3$ – (BCT) ceramics.

| Composition $(Ba_{0.70}Ca_{0.30})TiO_3$ | Maximum breakdown filed (kV/cm) | Discharge energy density $-(Ed)_d$ (J/cm$^3$) | Charge energy density $(Ed)_c$ (J/cm$^3$) | Energy storage efficiency (%) $(\eta = (Ed)_d/(Ed)_c)$ |
|---|---|---|---|---|
| Before aging | 50 | 0.20 | 0.35 | 58 |
| After aging | 50 | 0.24 | 0.39 | 61 |

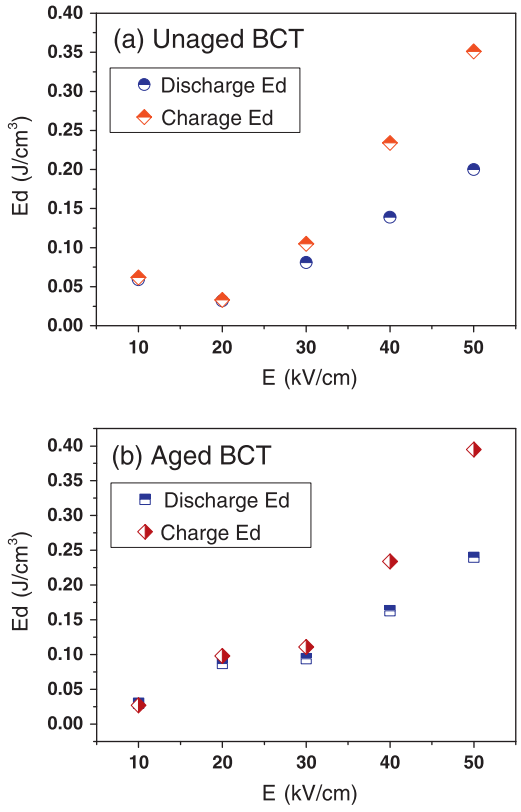


**Fig. 4.** Electric field dependent discharge curve and charge curve energy densities (before and after aging) of $(Ba_{0.7}Ca_{0.3})$ $TiO_3$ – (BCT) ceramics.

lower branch of *P–E* curve or discharged curve-upper branch of *P–E* curve) and *y*-axis is given by $Ed = \int E \cdot dP$, here *E* is applied electric field and P is polarization [29]. The stored energy can be estimated using polarization response under an applied electric field from polarization *P–E* loops, excluding the hysteresis losses. The ratio of discharge curve energy density $(Ed)_d$ to that of the charge curve energy density $(Ed)_c$ can be used to evaluate the energy efficient $(\eta = (Ed)_d/(Ed)_c)$ and to analyze the energy storage mechanism of the dielectric materials [30]. Higher energy densities can be obtained either by enlarging the difference between the saturation polarization and remnant polarization in the ferroelectric *P–E* loops or by enhanced electrical breakdown strength of the material.

The calculated discharge and charge curve energy densities and energy density efficiencies were listed in Table 2. The BCT ceramics exhibited energy densities ($\sim 0.2 - 0.39$ J/cm$^3$) and with high energy efficiencies ($\eta \sim 58$–61%) in both before and after aging than BCT ceramics, due to enhanced non-linear behavior of ferroelectric hysteresis loops. Enhanced energy storage properties in aged samples were attributed to antiferroelectric behavior in BCT ceramics. These moderate values of the energy densities might be due to low electric field strength (~50 kV/cm). Electric field dependent discharge and charge curve energy densities before and after aging were shown in Fig. 4(a) and (b). As the electric field increased from ~10 kV/cm to ~50 kV/cm, both discharge and charge curve energy densities were increased and the energy efficiency of storage capacitor is drastically increased to 61%.

## 4. Conclusions

In conclusion, based on the experimental observations, the BCT ceramics have shown tetragonal perovskite crystal structure along with orthorhombic $CaTiO_3$ peaks at room temperature due to incomplete solid solubility of $Ca^{2+}$ in $BaTiO_3$ lattice. The Raman spectrum at room temperature confirms the presence of tetragonal modes at room temperature. A strong $A_{1g}$ octahedral breathing mode was observed in BCT ceramics, which may be due to formation of oxygen vacancies at both $Ba^{2+}$ and $Ti^{4+}$ sites due to partial migration of $Ca^{2+}$ from $Ba^{2+}$ to $Ti^{4+}$ site. This may imply that the $Ca^{2+}$ ion is partially substituted for $Ti^{4+}$ in BCT ceramics and $O^{2-}$ vacancies have formed to compensate for the charge imbalance. However, to completely understand the site occupancy mechanism further the compositional analysis studies as well as the temperature dependent phase transitional studies are needed. Interesting aging induced double hysteresis like *P–E* loops were observed with higher saturation polarizations, which is also attributed to migration of oxygen vacancies (which are highly mobile) during aging. Bulk BCT ceramics with ferroelectric and piezoelectric behavior might be useful in actuator applications. Higher energy densities with high energy storage efficiencies were obtained for aged BCT ceramics which is due to antiferroelectric behavior. Optimizing intrinsic and extrinsic parameters (composition, bulk structure defect chemistry, microstructural development, thickness, electrode configuration and grain size and) will further improve dielectric breakdown values and enhance energy densities in making commercially viable energy storage device capacitors for wide range of energy storage applications.

## Acknowledgement

This work was supported by the National Science Foundation under Grant No: NSF-EFRI RESTOR # 1038272.

## Reference

[1] Venkata Sreenivas Puli, R. Martınez V, Ashok Kumar, J.F. Scott, Ram S. Katiyar, Mater. Res. Bull. 46 (2011) 2527–2530.
[2] Venkata Sreenivas Puli, Ashok Kumar, D.B. Chrisey, M. Tomozawa, J.F. Scott, Ram S. Katiyar, J. Phys. D Appl. Phys. 44 (2011) 395403.
[3] W. Liu, X. Ren, Phys. Rev. Lett. 103 (2009) 257602 (1–4).
[4] Z. Yu, C. Ang, R. Guo, A.S. Bhalla, J. Appl. Phys. 92 (2002) 1489.
[5] Zhi Yu, Chen Ang, Ruyan Guo, A.S. Bhalla, Mater. Lett. 61 (2007) 326–329.
[6] A. Dixit, S.B. Majumder, A. Savvinov, R.S. Katiyar, R. Guo, A.S. Bhalla, Mater. Lett. 56 (2002) 933–940.
[7] Lei Zhang, Om Prakash Thakur, Antonio Feteira, Gillian M. Keith, Andrew G. Mould, Derek C. Sinclair, Anthony R. West, Appl. Phys. Lett. 90 (2007) 142914.
[8] Liang-Yu Li, Xin-Gui Tang, Mater. Chem. Phys. 115 (2009) 507–511.
[9] Soonil Lee, Clive A. Randall, Appl. Phys. Lett. 92 (2008) 111904.
[10] J. Pokorny, U.M. Pasha, L. Ben, O.P. Thakur, D.C. Sinclair, I.M. Reaney, J. Appl. Phys. 109 (2011) 114110(1)–114110(5).
[11] Z.Q. Zhuang, M.P. Harmer, D.M. Smyth, R.E. Newnham, Mater. Res. Bull. 22 (1987) 1329.
[12] X. Ren, Nat. Mater. 3 (2004) 91–94.

[13] G.L. Yuan, Y. Yang, S.W. Or, Appl. Phys. Lett. 91 (2007) 122907.
[14] Z.Y. Feng, X. Ren, Appl. Phys. Lett. 91 (2007) 032904.
[15] T. Takanaka, K.I. Maruyama, Jpn. J. Appl. Phys. 30 (9B) (1991) 2236.
[16] Sining Yuna, Xiaoli Wang, Juanfei Li, Jing Shi, Delong Xu, Mater. Chem. Phys. 116 (2009) 339–343.
[17] Sining Yun, Xiaoli Wang, Jing Shi, Delong Xu, J. Mater. Res. 24 (10) (2009) 3073–3077.
[18] Sining Yun, Xiaoli Wang, Juanfei Li, Delong Xu, Phys. Status Solidi A 206 (2) (2009) 303–310.
[19] S. Tinte, K.M. Rabe, D. Vanderbilt, Phys. Rev. B 68 (2003) 144105.
[20] Desheng Fu, Mitsuru Itoh, Shin-ya-Koshiara, J. Phys.: Condens. Matter 22 (2010) 052204.
[21] Xusheng Wang, Hiroshi Yamada, Xu Chao-Nan, Appl. Phys. Lett. 86 (2005) 022905.
[22] M.R. Panigrahi, S. Panigrahi, Physica B 405 (2010) 1787–1791.
[23] Vidya S. Tiwari, Neelam Singh, Dhananjai Pandey, J. Am. Ceram. Soc. 77 (7) (1994) 1813–1818.
[24] Ronaldo Santos da Silva, Jean-Claude M'Peko, Lilian da Costa Fontes, Antonio-Carlos Hernandes, Mater. Res. 12 (3) (2009) 287–290.
[25] P. Victor, R. Ranjith, S.B. Krupanidhi, J. Appl. Phys. 94 (12) (2003) 7702–7709.
[26] R.C. De Vries, R. Roy, J. Am. Ceram. Soc. 3 (8) (1955) 142–146.
[27] M.C. Chang, S.C. Yu, J. Mater. Sci. Lett. 19 (2000) 1323–1325.
[28] S.E. Park, T.R. Shrout, J. Appl. Phys. 82 (1997) 1804.
[29] I. Burn, D.M. Smyth, J. Mater. Sci. 7 (1972) 339–343.
[30] Jilin Pan, Kun Li, Junjun Li, Tim Hsu, Qing Wang, Appl. Phys. Lett. 95 (2009) 022902.
[31] V. Krayzman, I. Levin, J.C. Woicik, F. Bridges, E.J. Nelson, D.C. Sinclair, J. Appl. Phys. 113 (2013) 044106.
[32] U.M. Pasha, H. Zheng, O.P. Thakur, A. Feteira, K.R. Whittle, D.C. Sinclair, I.M. Reaney, Appl. Phys. Lett. 91 (6) (2007) 062908.
[33] P.S.R. Krishna, D. Pandey, V.S. Tiwari, R. Chakravarthy, B.A. Dasannacharya, Appl. Phys. Lett. 62 (1993) 231–233.
[34] Antonio Feteira, Derek C. Sinclair, J. Mater. Chem. 19 (2009) 356–359.
[35] Tamsin Strathdee, Luke Luisman, Antonio Feteira, Klaus Reichmann, J. Am. Ceram. Soc. 94 (8) (2011) 2292–2295.